Solar flux variation of the electron temperature morning overshoot in the equatorial F region

Stolle, Claudia; Liu, H.; Truhlik, V.; Luehr, H.; Richards, P. G.

Published in:
Journal of Geophysical Research: Atmospheres

Link to article, DOI:
10.1029/2010JA016235

Publication date:
2011

Document Version
Publisher's PDF, also known as Version of record

Solar flux variation of the electron temperature morning overshoot in the equatorial *F* region

C. Stolle,[1] H. Liu,[2] V. Truhlík,[3] H. Lühr,[4] and P. G. Richards[5]

Received 22 October 2010; revised 7 January 2011; accepted 19 January 2011; published 12 April 2011.

[1] Using 8 years of CHAMP satellite observations of the equatorial electron temperature, T_e, we investigate its behavior during the morning overshoot and at ionospheric altitudes below 450 km including its variation with solar activity. The morning T_e has a maximum at the dip equator and decreases gradually with increasing latitude, which is due to the increasing importance of heat conduction as the dip angle becomes larger. The amplitude of the equatorial morning overshoot T_e decreases with increasing solar flux by about −10°K/solar flux unit depending on season and longitude. Trends of similar magnitude are predicted by the FLIP model. The model calculations confirm that the electron cooling due to enhanced electron-ion collisions increases faster than the heating of thermal electrons through collision with photoelectrons for increasing solar EUV. Both data and model showed that elevated electron temperatures persist to later local times during low solar activity. Obviously, the decreased background plasma density, together with the slower rise of electron density after sunrise under such conditions are responsible for the longer persistence. First investigations of longitudinal aspects revealed that the strength of the anticorrelation between morning T_e and solar flux and the seasonal difference of the T_e amplitude varies with longitude. The positive correlation between the morning overshoot and solar flux at 600 km as was shown earlier in Hinotori data is consistent with FLIP predictions and radar observations. The solar flux variation of the morning T_e reverses sign between 400 and 600 km.

Citation: Stolle, C., H. Liu, V. Truhlík, H. Lühr, and P. G. Richards (2011), Solar flux variation of the electron temperature morning overshoot in the equatorial *F* region, *J. Geophys. Res.*, *116*, A04308, doi:10.1029/2010JA016235.

1. Introduction

[2] The behavior of the *F* region electron temperature (T_e) is very complex depending on plasma and neutral density, neutral temperature and composition, plasma drift, the intensity and spectrum of the solar energetic flux, and on the shape of the geomagnetic field [e.g., *Schunk and Nagy*, 1978]. The understanding of the electron temperature is driven by ground based and satellite observations. Incoherent scatter radars have been a powerful tool in observing the low- and middle-latitude *F* region ionosphere at the radar locations and providing full local time and seasonal coverage [e.g., *Farley et al.*, 1967; *Otsuka et al.*, 1998; *Lei et al.*, 2007]. In situ satellite observations taken from Langmuir probes have importantly complemented the T_e database. In the 1960s and 1970s several satellites were launched [*Schunk and Nagy*, 1978, Table 3] and more recently the INTERCOSMOS family with launch dates in the 1980s and 1990s [*Truhlík et al.*, 2001]. These missions had perigees sometimes down to 200 km, but their apogees reached up to few thousand kilometers. The series of DMSP spacecrafts is in Sun-synchronous orbit at an altitude of ~850 km and Hinotori was flying in the 1980s in a circular orbit at 600 km. All of these satellites underwent extensive scientific exploitation [e.g., *Watanabe et al.*, 1996; *Ren et al.*, 2008; *Truhlík et al.*, 2003]. In this respect the multiyear CHAMP mission (2000–2010) with about 8 years of global and continuous T_e observations in a near-circular orbit between 450 and 300 km altitude provides a unique database.

[3] The electron temperature of the low-latitude *F* region ionosphere has a distinct daily variation. T_e is a few hundred Kelvin higher during sunlight hours than at night when $T_e \sim T_i \sim T_n$ [*Farley*, 1991; *Lei et al.*, 2007; *Truhlík et al.*, 2009], where T_n is neutral temperature. While the daytime and nighttime temperatures are rather stable, the temperatures have been found to be highly variable during sunrise hours. An electron temperature peak with values above 3000 K near 06 LT usually occurs at the dip equator and is well known as the morning overshoot. Following the first observations by *Evans* [1965] the phenomenon has been observed and modeled frequently [*Farley et al.*, 1970;

[1]National Space Institute, Technical University of Denmark, Copenhagen, Denmark.
[2]Research Institute for Sustainable Humanosphere, Kyoto University, Kyoto, Japan.
[3]Institute of Atmospheric Physics, Academy of Sciences of the Czech Republic, Prague, Czech Republic.
[4]Helmholtz Centre Potsdam, GFZ German Research Centre for Geosciences, Potsdam, Germany.
[5]Department of Physics and Astronomy, George Mason University, Fairfax, Virginia, USA.

0148-0227/11/2010JA016235

Watanabe and Oyama, 1996; *Su et al.*, 1995; *Oyama et al.*, 1996].

[4] The mechanism to produce the morning overshoot was first proposed by *Da Rosa* [1966]. The temperature overshoot occurs because the heating rate is approximately linear in the electron density while the cooling rate is quadratic in the electron density. The electron heating depends on the electron density, because the primary heat source for the thermal electrons is by collision with the photoelectrons that are generated by the photoionization of the neutral gases [*Schunk and Nagy*, 1978, Figure 2]. The photoelectron flux increases linearly with solar activity. It is important to note that the overall photoelectron flux is not sensitive to the neutral composition [*Richards and Torr*, 1985]. The loss rate is approximately quadratic in electron density because the electron density is approximately equal to the O^+ density in the F2 region [*Schunk and Nagy*, 1978, equation 47]. Above ~250 km altitude, the measured photoelectron flux shows little diurnal variation for solar zenith angles below ~95° [*Lee et al.*, 1980]. On the other hand, the photoionization rate does not peak until the solar zenith angle is less than 90°. Thus, the electron heating occurs promptly at sunrise, but the build up of ionization is more gradual so that the cooling by ions is delayed and this allows for a fast rise in T_e. *Oyama et al.* [1996] proposed that strong downward plasma drift velocities further decrease the local ion density, which increases T_e. As the ion density builds up after sunrise, T_e decreases to daytime values that are reached at about 09 LT. The neutral density and the electron-neutral cooling rate also build up after sunrise but it has a smaller effect on the electron temperature than the plasma density. The high temperatures are not seen in the evening during sunset because the electron density has not had time to decay from the high daytime values.

[5] A variation of the equatorial morning overshoot with increasing solar activity, so increased EUV flux, was observed by the Hinotori satellite at 600 km altitude. *Watanabe and Oyama* [1996] reported higher amplitudes of the morning overshoot electron temperature at equatorial latitudes at solar flux indices $F10.7 > 250$ than for $F10.7 < 150$, and *Oyama et al.* [1996] got similar results when grouping the data in $F10.7 > 175$ and $F10.7 < 200$.

[6] Recently, investigations on presunrise enhancements of the plasma temperatures based on ion temperatures measured on board the ROCSAT-1 satellite and modeling results [*Chao et al.*, 2010] and on the Hinotori satellite data [*Kakinami et al.*, 2010] has been performed for an altitude of 600 km for low and midlatitudes. They found a pronounced latitudinal asymmetry of temperature enhancement before sunrise depending on season. The heating was explained by photoelectrons streaming along the field line from the sunlit magnetic conjugate ionosphere. The seasonal asymmetry is caused by the declination of the Earth's magnetic field. However, for altitudes of the CHAMP satellite, photoelectron transport is not important at the dip equator because the photoelectrons are confined by the horizontal magnetic field. Local heating and cooling dominates and the morning overshoot starts at sunrise.

[7] The CHAMP satellite provides a new and unique opportunity to investigate the ionospheric behavior at altitudes between 300 km and 450 km over a multiyear period. We will investigate the variations of the electron temperature including its solar flux dependence at equatorial latitudes and sunrise hours and compare our results with model predictions and other available observations.

2. Data and Model

2.1. CHAMP Data

[8] The CHAMP (Challenging Minisatellite Payload) satellite was launched on 15 July 2000 into a near-circular, near-polar (inclination = 87.3°) orbit with an initial altitude of about 450 km [*Reigber et al.*, 2002]. Its orbital height decayed to 150 km when the successful mission ended with the reentry of the satellite into the atmosphere on 19 September 2010. Successive satellite passes were separated by 23° in geographic longitude. The progress in local time was about 5.5 min per day, thus one full local time coverage was obtained in ~130 days. The instrument of particular interest for this study is the Planar Langmuir Probe (PLP). The PLP performs a 1 s sweep every 15 s to determine the in situ plasma density and electron temperature. Details of the retrieval of electron density and temperature from the PLP observations are given by *McNamara et al.* [2007] and *Cooke et al.* [2003].

[9] The CHAMP PLP electron density readings have frequently been used in scientific investigations, e.g., of the low and equatorial latitudes [*Liu et al.*, 2007; *Stolle et al.*, 2008; *McNamara et al.*, 2010]. *McNamara et al.* [2007] have compared the CHAMP electron density values with plasma frequency measurements of the Jicamarca digisonde located at 11.95°S, −76.87°E (geographic), and ~1°N (geomagnetic). For CHAMP orbit heights below the F2 peak they report an average discrepancy between the PLP and digisonde records of only 4%, with a standard deviation of 8.8%. At heights above the F2 peak a mean difference of 2.6% (standard deviation 13.3%) is given. Such discrepancies lie within the uncertainty of the digisonde measurements and the applied electron density retrieval technique.

[10] The CHAMP electron temperature observations have not been fully exploited so far and the first comparison studies with independent data have been reported recently by *Rother et al.* [2010]. These comparisons are performed at two incoherent scatter radar sites, Arecibo (18.3°S, −66.75°E (geographic), ~30°N (geomagnetic)) and Tromsø (69.6°N, 19.2°E (geographic), 66.7°N (geomagnetic)). *Rother et al.* [2010] found that due to an unfavorable PLP setting, the retrieved CHAMP T_e data are severely biased before 19 February 2002. In order to improve attitude stability, the CHAMP satellite was rotated by 180° about the yaw axis on 22 February 2010. From that date on electron density and temperature measurements could no longer be performed reliably. After a post-processing calibration of T_e, *Rother et al.* [2010] reported a small average deviation of the CHAMP data from Arecibo data of 1.2% (standard deviation 8.3%) and from Tromsø data of 4.1% (standard deviation 8.4%). This post-processing calibration consists of a latitudinal/longitudinal variable bias, which was found by different ascending and descending orbit nodes. After removal of this bias, good agreement was achieved with Areceibo data. However, at the time of publication, they could not provide an explanation for the source of the difference between ascending and descending nodes. Our study concentrates on the equatorial region (±5° magnetic latitude)

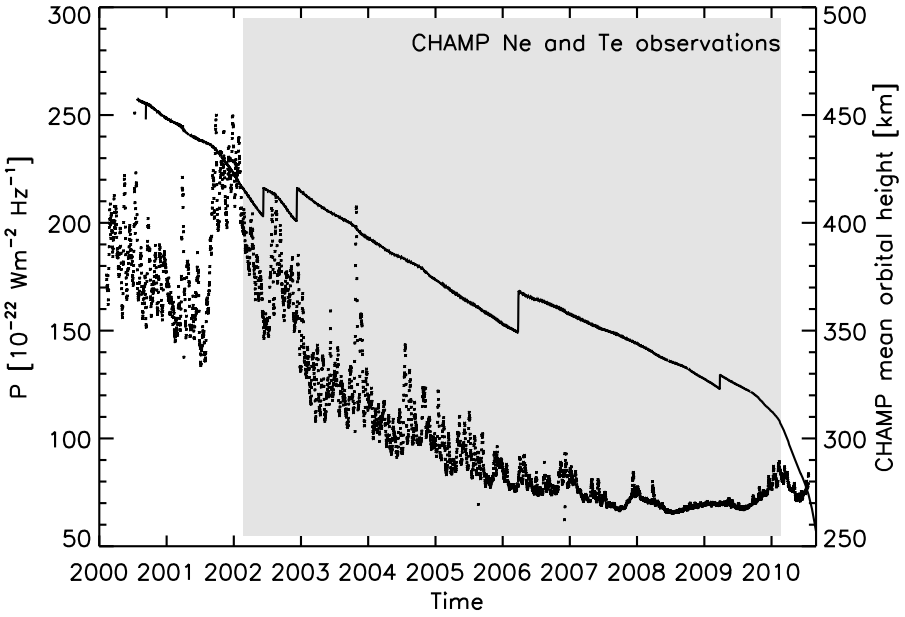

Figure 1. Temporal evolution of the solar flux index P (dots) and the CHAMP mean orbit altitude (solid line). The shaded area indicates the time of available T_e observations. Ticks every year mark 1 January.

where the difference between ascending and descending orbits is nearly zero [*Rother et al.*, 2010, Figure 8].

[11] The CHAMP satellite orbit decayed by more than 100 kilometers between launch in 2000 and February 2010. Figure 1 shows the mean orbital altitude of CHAMP and the solar flux proxy P[10^{-22} Wm^{-2} Hz^{-1}] = (F10.7 + F10.7A)/2 [*Richards et al.*, 1994], where F10.7A is the 81 day average of the F10.7 values centered on the day of interest. Since the satellite altitude and the solar flux both decayed during the mission, it is possible to build three different groups of CHAMP observations, which are each assigned to a solar flux and altitude range. Table 1 displays the number of observations, altitude and solar flux distributions for the three data groups. Some observations with P > 80 appear at altitudes below 320 km. These observations can clearly be attributed to the end of the mission in 2010 when the solar flux is rising again. These data have not been included in the analysis in order to preserve the solar flux/altitude relation in the groups. To avoid the contribution from sounding different heights when analyzing, e.g., solar flux variations, CHAMP electron density observations have often been normalized to a common altitude using ionospheric models [e.g., *Liu et al.*, 2007; *Stolle et al.*, 2008]. Since empirical modeling of electron temperature is not yet as advanced as for electron density, we avoid introducing an additional uncertainty in the data by, for example, scaling to a common height with model predictions. Instead, we remind the reader of the different sampling altitudes to consider also the different solar flux levels.

2.2. FLIP Model

[12] The field line interhemispheric plasma (FLIP) model is a one-dimensional (1-D) model that calculates the plasma densities and temperatures along entire magnetic flux tubes from below 100 km in the Northern hemisphere through the plasmasphere to below 100 km in the Southern hemisphere. The model uses a tilted dipole approximation to the Earth's magnetic field [*Richards*, 2001, 2002].

[13] The equations solved are the continuity and momentum equations for O^+, H^+, He^+, and N^+ and the energy equations for ion and electron temperatures. The equations are solved using a flux-preserving formulation together with a Newton iterative procedure that has been described by *Torr et al.* [1995]. Electron heating due to photoelectrons is provided by a solution of the two-stream photoelectron flux equations using the method of *Nagy and Banks* [1970]. The photoelectron solutions have been extended to encompass the entire field line on the same spatial grid as the ion continuity and momentum equations. Chemical equilibrium densities are obtained for NO^+, O_2^+, N_2^+, $O^+(^2P)$, and $O^+(^2D)$ ions below 500 km altitude in each hemisphere. The densities of minor neutral species NO, $O(^1D)$, $N(^2D)$, and $N(^4S)$ are obtained by solving continuity and momentum equations from 100 to 500 km in each

Table 1. Number of Observations, Solar Flux, and Altitude Distribution for Three Discrete Groups of CHAMP Data Sorted by Solar Flux Level

P Range	Mean P	Number of Observations (±5° Dip Latitude)	Mean Altitude	Standard Deviation	Lowest Altitude	Highest Altitude
<80	73	340,137	340.3 km	15.3 km	308.0 km	371.7 km
80 ≤ P < 130	100	236,271	378.2 km	19.2 km	342.0 km	418.3 km
130 ≤ P	165	135,610	409.7 km	10.8 km	380.5 km	440.2 km

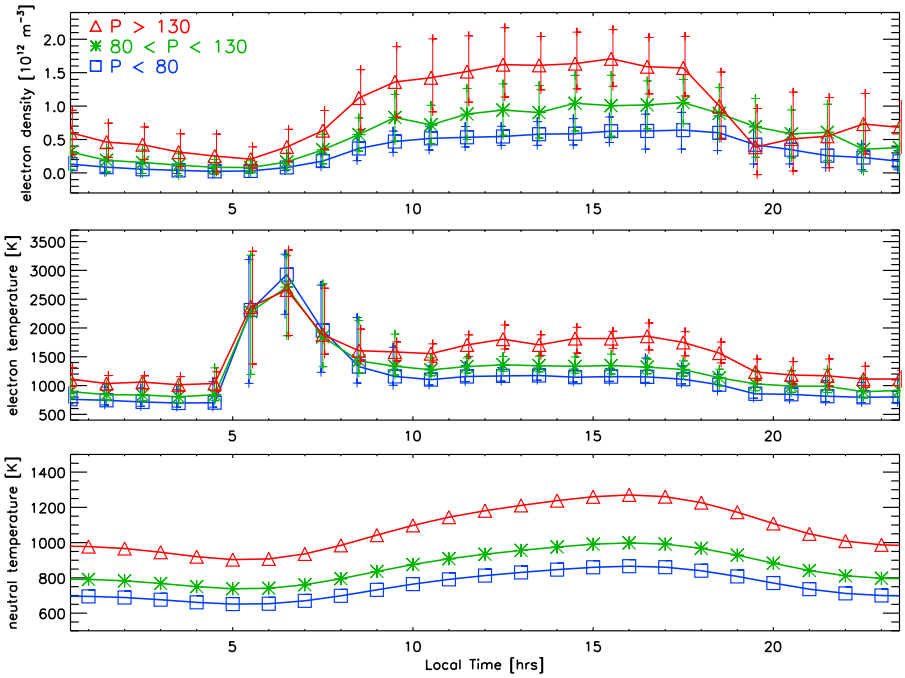

Figure 2. Diurnal variation of CHAMP (top) electron density and (middle) electron temperature data between ±5° dip latitude for three different solar flux levels averaged over longitude and season. Standard deviations of the mean values are shown as thin vertical lines. For better visibility the standard deviations for the different solar flux levels are drawn slightly displaced in local time. (bottom) Neutral temperature estimations from the NRLMSISE-00 model.

hemisphere. The model also has the capability of solving for the first five excited states of vibrationally excited N_2 that can significantly increase the $O^+ + N_2$ reaction rate.

[14] The solar EUV fluxes are important because they are not only responsible for the ionosphere but also for the photoelectrons that heat the thermal electrons. The FLIP model uses the EUV model for aeronomic calculations (EUVAC) for the solar EUV fluxes [*Richards et al.*, 1994]. *Richards et al.* [2006] showed that the EUVAC model fluxes are consistent with recent satellite measurements.

[15] The primary heat source for thermal electrons is the photoelectron flux, which is calculated by the FLIP model from the solar EUV fluxes [*Richards et al.*, 2006]. There is an additional source of electron heat from electron quenching of N(2D) [*Richards*, 1986]. The FLIP model ion-neutral cooling rates are from *Schunk and Nagy* [1978]. The 3 main cooling processes of thermal electrons are (1) Coulomb collisions with ions, (2) fine structure excitation of atomic oxygen, and (3) vibrational excitation of N_2. There is cooling by vibrational excitation of O_2 as well as rotational excitation of O_2 and N_2 and excitation of O(1D) but these are minor above 250 km. The FLIP model electron-ion cooling rate is from *Itikawa* [1975]. For this study the model chemical reaction rates have been updated to those published by *Fox and Sung* [2001].

[16] For the neutral atmosphere the FLIP model uses the revised MSIS model, NRL Mass Spectrometer, Incoherent Scatter Radar Extended model (NRLMSISE-00) [*Picone et al.*, 2002]. The NRLMSISE-00 model O_2 densities are not much different at solar minimum but they are a factor of 2 smaller than in previous MSIS models [*Hedin*, 1987] at solar maximum. Recently the FLIP model was improved by inclusion of the E × B drift. For this study values of E × B drift were taken from *Scherliess and Fejer* [1999].

3. Observations

[17] Before discussing the CHAMP equatorial electron temperature observations in more detail, Figure 2 shows the diurnal variation of hourly means of electron density and temperature at equatorial latitudes for low, medium and high solar flux levels. The provided standard deviations in this paper are calculated as the standard deviation of the data points lying below the total mean and a standard deviation of the data points lying above the total mean. The total mean, represented by a thick line, is derived from all data points before calculating the upper and lower standard deviations. The electron density is low during the night, and increases between about 06 LT and 10 LT to the daytime values. N_e is higher for higher solar flux, except after sunset between 18 LT and 22 LT. The very low densities for high solar flux result from the equatorial plasma fountain, which is increased due to the prereversal enhancement of the eastward electric field after sunset. This process creates an important trough above the equator, which was seen in CHAMP data by *Liu et al.* [2007]. The evening density decreases with increasing solar flux activity because the prereversal enhancement of plasma drift increases with solar activity [*Fejer et al.*, 2008].

[18] Figure 2 (middle) displays local time profiles of CHAMP electron temperatures at the dip equator. T_e values range between 600 K to 1000 K at night and 1200 K and 1800 K during daytime. T_e relaxes to the neutral temperature at night in the absence of electron heating while during the

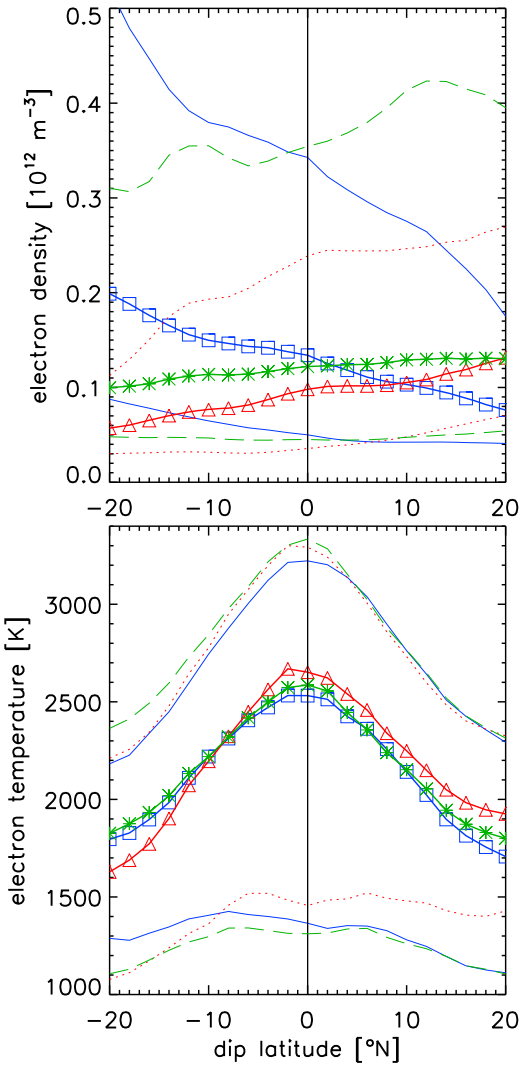

Figure 3. Latitudinal profiles of CHAMP (top) N_e and (bottom) T_e for a time window between 05 and 07 LT (averages over all longitudes). The red line (triangles) shows observations from May, June, and July (thin dotted lines show standard deviations); the green line shows observations (asterisks) from February, March, April, August, September, and October (standard deviation: thin dashed lines); and the blue line shows observations (squares) from November, December, and January (standard deviation: thin solid lines).

day T_e is only a few hundred degrees higher than T_n because of the high electron-ion cooling rates. Since the neutral temperature increases with solar activity, this helps to explain the increase in T_e with increasing solar activity. The positive correlation of electron temperature with solar flux level was shown with other radar and satellite data at equatorial and low latitudes [*Watanabe and Oyama*, 1996; *Lei et al.*, 2007; *Truhlík et al.*, 2009], as well as the increased ratio between day and night time T_e [*Watanabe and Oyama*, 1996]. T_e begins to increase near 05 LT, rises to a peak of about 3000 K near 06 LT and then decreases to daytime values by 09 LT. The elevated temperatures occur because the heating rate by far exceeds the cooling rate at this time. This phenomenon is well known as the morning overshoot. In contrast to the increase of the electron temperature at all other local times, the line representing lowest P values exceeds the other solar flux levels in temperature, suggesting a negative trend of the morning overshoot with increasing solar activity. Around sunrise, the scatter in the data increases markedly compared to daytime or nighttime because the morning overshoot depends on the background plasma density, on neutral temperature, on composition, and the neutral wind which all have large day-to-day variability. An increased data scatter near the equator for local times around 06 LT was also found in Hinotori observations by *Kakinami et al.* [2010, Figure 2]. CHAMP does not provide neutral temperature observations. To verify the nighttime and daytime relation between neutral and electron temperature, Figure 2 (bottom) provides NRLMSISE-00 [*Picone et al.*, 2002] predictions of neutral temperature. The model was run for the three mean solar flux levels and altitudes as displayed in Table 1, and for $Ap = 7$. For each local time hour, the model was run for each 15th of a month and for every 10° of longitude at the dip equator to generate seasonal/longitudinal averages as is displayed from the CHAMP data. CHAMP T_e and modeled T_n are close to each other during night and are only few 100 K separated during day.

[19] Figure 3 shows longitudinal averages of CHAMP N_e and T_e versus magnetic latitude over the 05 LT to 07 LT time window when the morning overshoot is most pronounced, as seen in Figure 2. This also explains the large data scatter. A method to estimate the significance of the calculated mean is by dividing its standard deviation by the square of the number of involved data points, e.g., $SD/\sqrt{n}$, where SD is standard deviation and n is the number of observations per bin. The uncertainty of the standard deviations is only about ±20 K for T_e and $\pm 0.5 \times 10^{10}$ m^{-3} for N_e. Therefore, the displayed trends are significant. The colors and line styles denote different seasons; December solstice months are represented by November to January (NDJ, blue/squares), June solstice months are from May to July (MJJ, red/triangles), and the equinox months are February to April and August to October (FMA and ASA, green/asterisks). For these three curves the mean altitudes are 360 km, 362 km, and 364 km, and the mean solar flux indices P are 100, 91, and 102, respectively. At low, nonequatorial latitudes, the electron density is higher in the summer hemisphere. Around the dip equator, it is lowest during June solstice months and highest during December solstice months. This is in accordance with recent publications which found a yearly global minimum in the low-latitude electron and neutral densities during June solstice [*Liu et al.*, 2009; *Müller et al.*, 2009]. At the dip equator the seasonal means of morning electron density and temperature are anticorrelated. At all three seasons, the averaged maxima of the temperatures occur at the dip equator and the latitudinal shape of the morning T_e is similar, e.g., no significant displacement toward southern or northern latitudes is visible. This indicates that we don't misinterpret the T_e behavior when we select CHAMP observations around the dip equator and when we look at different seasons. The dip latitudinal variation is clearly not due to variation in the local heating or cooling rates because it does not show any relationship with the electron density. The decrease in T_e with dip latitude

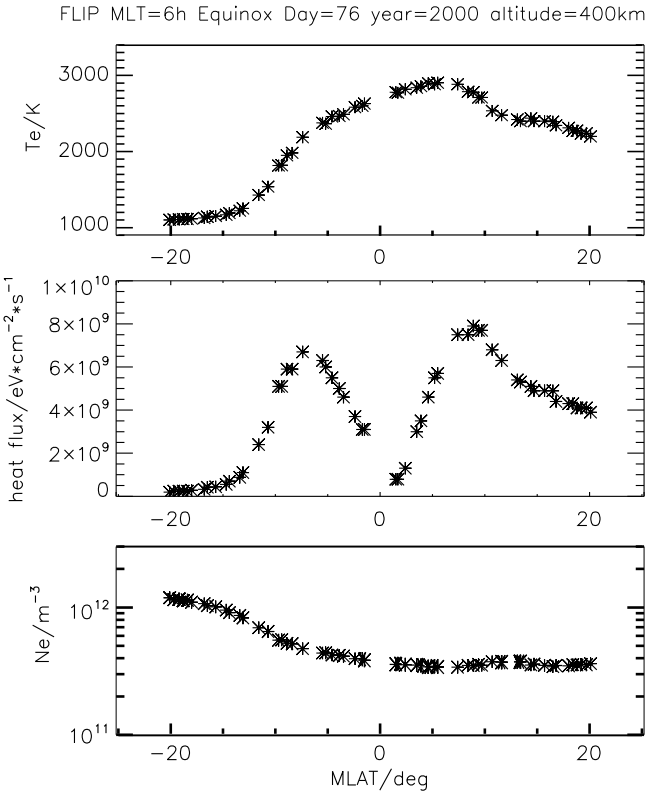

Figure 4. Latitudinal profile of FLIP electron density, heat flux, and electron temperature calculated for 1 day at the longitude of Jicamarca and at 400 km altitude. Time of calculation is given.

shown in Figure 3 is due to the increasing importance of heat conduction as the dip angle increases away from the equator. Here, local heating or cooling rates may play a secondary role. Heat conduction is reduced at the dip equator because of the horizontal magnetic field geometry. Figure 4 shows FLIP model results of the latitudinal distribution of electron density, heat flux and electron temperature at an altitude of 400 km at the longitude of Jicamarca for one arbitrary day in 2000. The model confirms a minimum of heat conduction in the region of horizontal field lines. At about 10° magnetic latitude where the model predicts largest heat flux the electron temperature decrease is also enhanced. It should be noted that heat conduction, contributing either to cooling or heating, is only important for low-electron densities like those shown in Figure 3 [see also, *Geisler and Bowhill*, 1965]. For high-electron densities, local cooling dominates cooling contributions from heat conduction. In analogy, FLIP heat flux is again reduced when electron density gets high, e.g., above 1×10^{12} m^{-3}. Since these model results don't represent a climatology, but were calculated for one arbitrary day, the profiles of the result parameters can vary with different conditions, but this example confirms our suggestion of reduced heat conduction at the dip equator.

[20] Figure 5 shows the longitudinal variation of the morning electron temperature and density measured by CHAMP for different seasons for solar flux level $P < 80$ where the CHAMP data distribution is most complete and the altitude was near 340 km. The lines represent data averages between 04.5 and 09 LT. The time window was chosen to include the morning T_e temperature rise, maximum, and decline for all seasons (see below, e.g., Figure 6) and therefore avoids biasing that might occur with shorter local time windows. An averaged value has been derived for geographic longitudes separated by 30° longitude and using a centered sliding window of 60°. Due to the wide longitudinal window and the local time window including the morning overshoot, the data scatter is large, but the uncertainty of the standard deviation is only about ±30 K for T_e and $\pm 0.5 \times 10^{10}$ m^{-3} for N_e. The morning equatorial electron densities and temperatures are not uniform over season and longitude. The electron density is lowest during June solstice months at almost all longitudes which confirms findings from Figure 3. At first sight, the corresponding electron temperature data are anticorrelated to the density in each season. The correlation coefficients for the months MJJ and FMA_ASO are −0.91 and −0.95, respectively. Electron

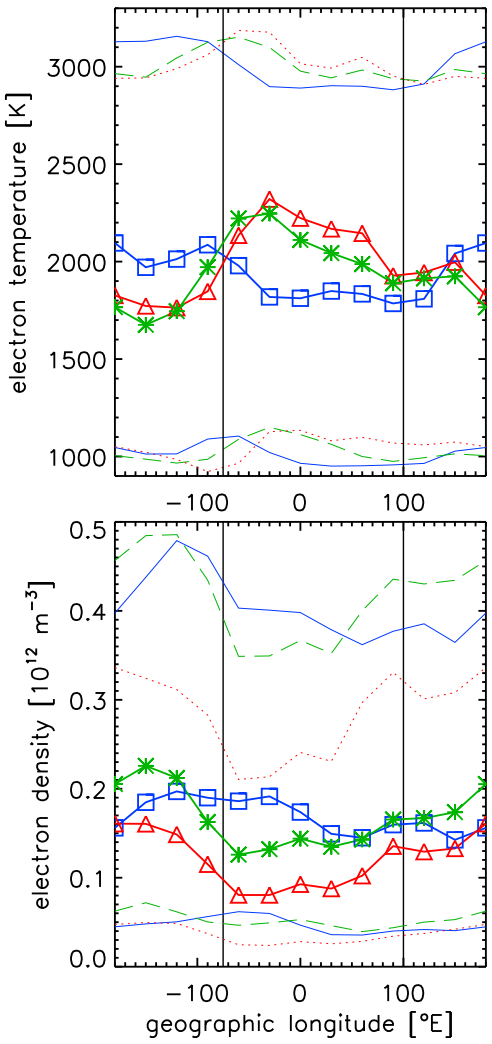

Figure 5. Longitudinal profiles of CHAMP equatorial electron temperature and density data averaged between 04:30 LT and 09 LT for solar flux indices $P < 80$. The vertical lines mark the −75°E and 100°E longitudes. The thin lines indicate the standard deviation for each season. Color and line codes same as Figure 3.

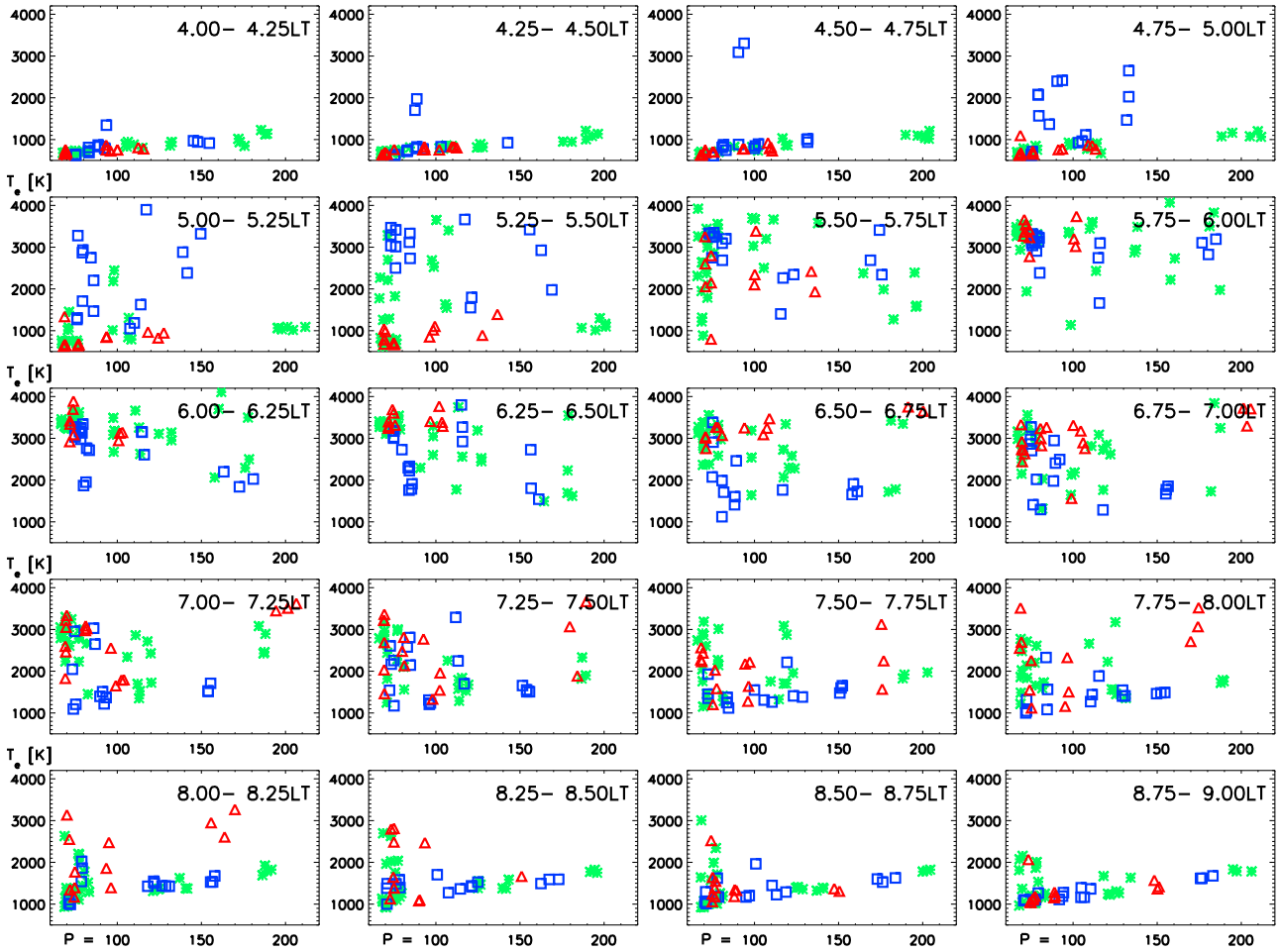

Figure 6. CHAMP T_e observations plotted versus solar flux index P at 15 min increments around the morning overshoot (data are averaged over longitudes between −90°E and −60°E). Local time intervals are displayed top right in each panel in decimal hours. Red triangles are associated to observations from May, June, and July; green asterisks are associated to February, March, April, August, September, and October; and blue squares are associated to November, December, and January.

density and temperature in NDJ months seem also to be anticorrelated locally, e.g., between −180° and −100°E, but the overall correlation coefficient is only 0.1. At the moment, we cannot explain this difference from the other seasons. However, we can observe that the longitudinal variation of T_e follows closely the longitudinal variation of equatorial N_e underlining the close relation of the equatorial electron temperature to the plasma density.

[21] Since the main focus of this study is the solar flux behavior of the morning T_e, Figure 6 shows the electron temperatures plotted against the solar flux index P between −90°E and −60°E geographic longitude. Each panel includes data of a 15 min local time window. At 04 LT, the T_e values are well organized with increasing solar flux, irrespective of the season. The blue squares (NDJ) rise first to high values. After 05 LT the green asterisks (FMA and ASO) follow and finally the red triangles (MJJ) gain also high values. The difference in the start of the morning overshoot can easily be explained by the local time variation of the solar zenith angle with season. During NDJ months the dip equator at South America lies in the summer hemisphere. Correspondingly, the end of the morning overshoot happens earliest for December solstice months. At 09 LT the data is again well organized with increasing solar flux except for few data points at low solar flux numbers being still elevated.

[22] To investigate the correlation of the morning overshoot temperatures measured by CHAMP we apply a linear fit to the data. Since the distribution of the CHAMP data over solar flux also includes some contributions from the altitudinal T_e variations due to the altitude decay of the satellite, a "quiet time baseline" is subtracted from the observations before performing correlations between T_e and P. The "quiet time baseline" is retrieved from the linear regression of the observations between 04 LT and 04:15 LT, just before the morning overshoot starts (upper left panel in Figure 6). Using the slope from this panel, which is here 3.37 K/solar flux unit (sfu), we normalize each observation, i, also in all other panels to a fixed P value, P^{norm}, by $T_e^{norm}(i) = T_e(i) + [3.37\ \mathrm{K/sfu}(P^{norm} - P(i))]$. The analysis is insensitive to the chosen P^{norm}. By that we eliminate the uncertainty due to the altitude decay in the correlation study and we normalize for the temperature increase of the background ionosphere with increased solar flux index P. Therefore, the following

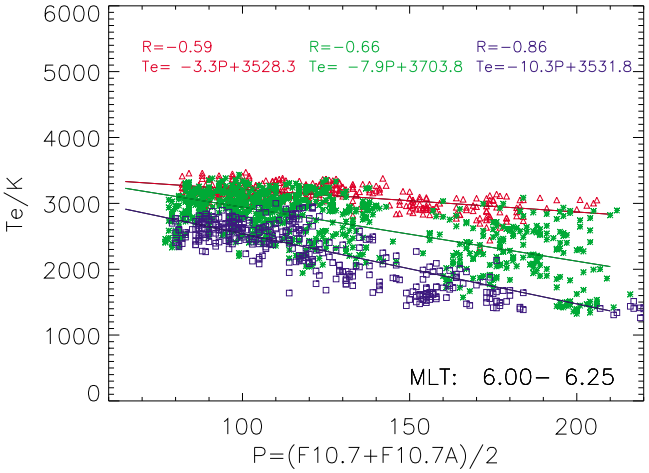

Figure 7. FLIP model T_e results at 350 km altitude plotted versus the solar flux index P between 6:00 and 6:15 LT and at Jicamarca longitude. Color and line codes same as Figure 6.

analysis describes the amplitude of the morning overshoot rather than the absolute T_e values. The slopes of the regression lines from the baseline data in the subsequent panels are negative during the morning overshoot. E.g., for the 6.00 LT to 6:15 LT window, where we expect the overshoot to occur at all seasons, the slopes are −14.2 K/sfu (correlation coefficient = cc = −0.93) for NDJ, −7.4 K/sfu (cc = −0.55 for FMA and ASO, and −16.0 K/sfu (cc = −0.68) for MJJ.

4. Results and Discussion

4.1. Solar Flux Dependence

[23] The CHAMP satellite has provided the possibility to observe the equatorial ionospheric F region at local times of the morning overshoot. These observations shall be compared with previous findings and discussed in comparison with model results. Although the data scatter is high, we found an inverse correlation of the amplitude of the morning overshoot with solar flux. To verify our observations we performed FLIP model simulations for the observational conditions in terms of local time, location, day of year, and solar flux level. The model has been run for each day between 1 January 2002 until 31 December 2005. The shorter FLIP interval than the CHAMP observation interval has been chosen as a compromise considering the expensive model running time and a wide coverage of solar flux indices $80 < P < 230$ between 2001 and 2005. Figure 7 shows the FLIP model results of T_e over solar flux for different seasons, at 350 km, at about −75°E (Jicamarca longitude), and between 06–06:15 LT. The slope values derived from the absolute, nonbaseline temperatures are provided within Figure 7. When applying baseline model results (to make it comparable with results derived from CHAMP observations) the slopes are −13.1 K/sfu for NDJ, −8.7 K/sfu for FMA and ASO, and −5.0 K/sfu for MJJ. The model results predict a negative correlation with solar flux for all seasons, for both the absolute temperatures and the amplitude of the morning overshoot. The slopes are in the same order as derived from the observed temperatures. In both, data and model, the anticorrelation is stronger in December solstice than during equinox. The shallowest slope is predicted by FLIP during June solstice, but a steeper slope has been derived from the data. However, this regression was performed from data only for low solar flux conditions; unfortunately, no data for high solar flux is available between 05:45 LT and 06:30 LT, which makes the regression from CHAMP data for June solstice not very representative.

[24] The mechanism of the morning overshoot has been described in the introduction. In the following, we want to discuss the negative correlation of the overshoot electron temperatures with solar flux. The photoelectron flux increases linearly with solar activity. There is a factor of 2–3 solar cycle variation in both the measured and modeled ionospheric photoelectron flux [*Richards and Peterson*, 2008]. Therefore, with increasing solar activity level, there will be an increase in electron heating of a factor of 2–3 due to the increased photoelectron flux as well as an approximate linear increase related to the increased electron density. This increased heating is opposed by increased cooling, which is primarily due to increased electron-ion cooling which is about quadratic in the electron density. Note that, above 300 km, 80% or more of the model cooling rate results from electron-ion cooling. To evaluate solar activity related changes to this balance, Figure 8 shows the ratio between FLIP T_e cooling and heating rates over local time, during the equinox months and for three different solar flux levels ($P > 140$, $90 > P > 140$, and $P < 90$). Clearly, electron heating dominates cooling between 05 LT and 06 LT and its ratio (heating/cooling) increases with decreasing solar flux. The model results show that the cooling rate, which is quadratic in the electron density, increases more rapidly with solar activity than the combined increases in the heating rate due to the linear increases in the photoelectron flux and the electron density.

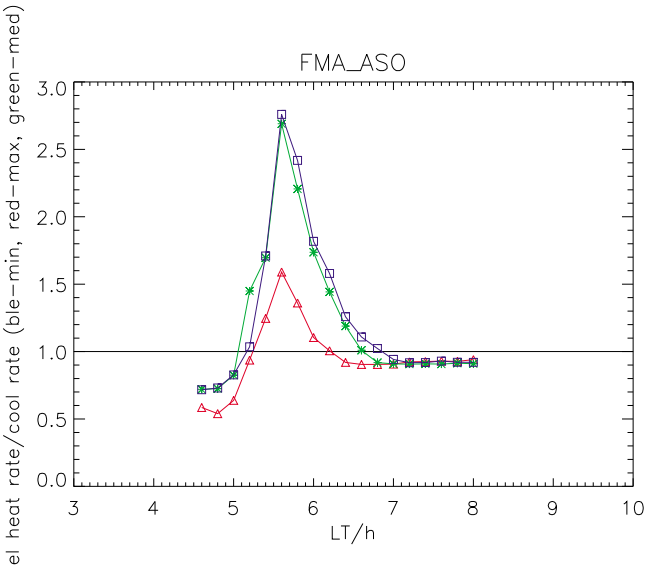

Figure 8. Ratios between electron heating and cooling rate as calculated by the FLIP model for equinox conditions and at 350 km altitude and Jicamarca longitude. Red (triangles), $P > 140$; green (asterisks), $90 > P > 140$; and blue (squares), $P < 90$.

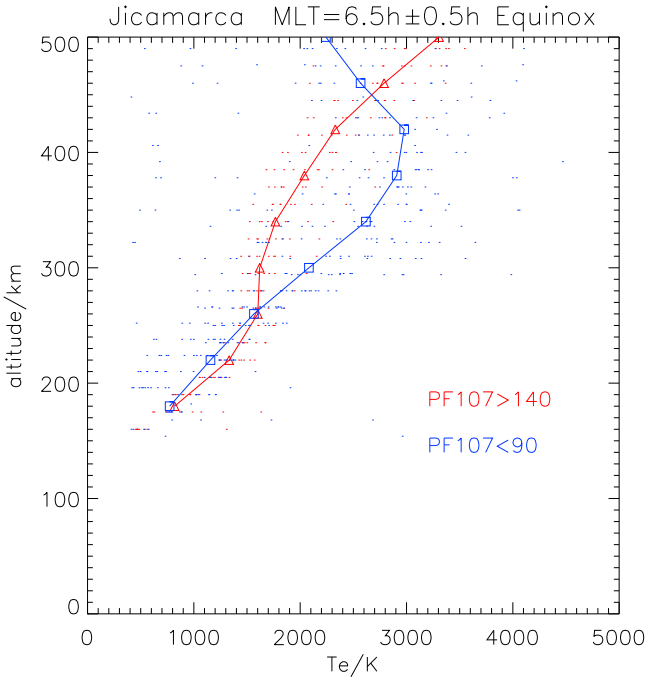

Figure 9. Averaged altitude profiles of electron temperature measured around 06 LT by the Jicamarca incoherent scatter radar for solar flux levels $P > 140$ (red, triangles) and $P < 90$ (blue, squares).

[25] However, at an altitude of 600 km, *Watanabe and Oyama* [1996] and *Oyama et al.* [1996] observed higher morning overshoot amplitudes during high solar activity than for low solar activity. To investigate this altitude difference in more detail, Figures 9 and 10 show the vertical profiles of electron temperature at around 06 LT as measured by the Jicamarca incoherent scatter radar and derived from the FLIP model. FLIP was run for altitudes 300, 350, 400, and 500 km. In the altitude range between 300 km and 400 km (CHAMP altitudes), the electron temperature during low solar flux years is higher than during high solar flux years which is in agreement with Figure 7. At 500 km altitude this trend is reversed and temperatures are lower during low solar flux. Comparing the FLIP predictions with Jicamarca incoherent scatter observations, the curves have similar shape in model and data, but the amplitudes are slightly overestimated by FLIP by a few 100 K. Provided the positive correlation between T_e and solar flux level holds until the height of 600 km, the FLIP model and the radar data confirm the positive correlation of the morning overshoot amplitude with solar flux at Hinotori altitudes. Significant differences between the two ionospheric altitudes are at 600 km (1) the neutral and plasma density is lower and (2) a longer part of the local magnetic field lines lies in the ionosphere. These circumstances may shift the balance between the local electron heating and cooling rates and photoelectron transport may become more important. This has to be verified in subsequent modeling studies.

[26] Another variable of the morning overshoot with solar activity is the duration of elevated electron temperatures. Figure 6 shows that the temperature stays high for later local times during low than during high P values because the electron density ramps up more slowly for low P. E. g., after 08.25 LT T_e already shows a positive correlation with solar flux as is expected for the dayside for $P > 100$, but for $P < 100$ the data points are still scattered. Similarly in Figure 2, T_e seems to reach its daytime equilibrium around 08 LT for $P \geq 130$ (the data scatter is reduced considerably), but it is only around 10 LT for $P < 80$. Such behavior is confirmed by the FLIP model. Figure 11 provides the local time evolution of T_e for the Jicamarca longitude at an altitude of 350 km for equinox months. The restoration of the equilibrium to daytime T_e values occurs later for low solar flux (~08 LT) than for high solar flux (~07 LT). This is in accordance with the behavior of the ratio between cooling and heating derived from the FLIP model (Figure 8). The time interval for which the cooling/heating rate ratio is above 1 is shorter for high solar activity than for medium or low solar activity. The ratio of cooling/heating reaches 1 about 1 h earlier than the daytime equilibrium is reached in the data. Calculating the mean slopes of the N_e increase between 5.5 LT and 8.5 LT from Figure 2 gives 1.1×10^5 cm^{-3} h for $P < 80$, 1.7×10^5 cm^{-3} h for $80 \leq P < 130$, and 2.99×10^5 cm^{-3} h for $P \geq 130$. Both the higher background electron density and the steeper rise of the electron density during solar active years are likely to be responsible for the shorter duration of the morning overshoot.

4.2. Longitudinal Aspects

[27] The solar flux dependence of the morning overshoot at about 350 km altitude has been obtained for longitudes of −90° to −60°E where the magnetic declination ranges between 10° and −10°. Although the longitudinal variation of the morning overshoot is not the main subject of this paper, we want to determine if our findings also hold at

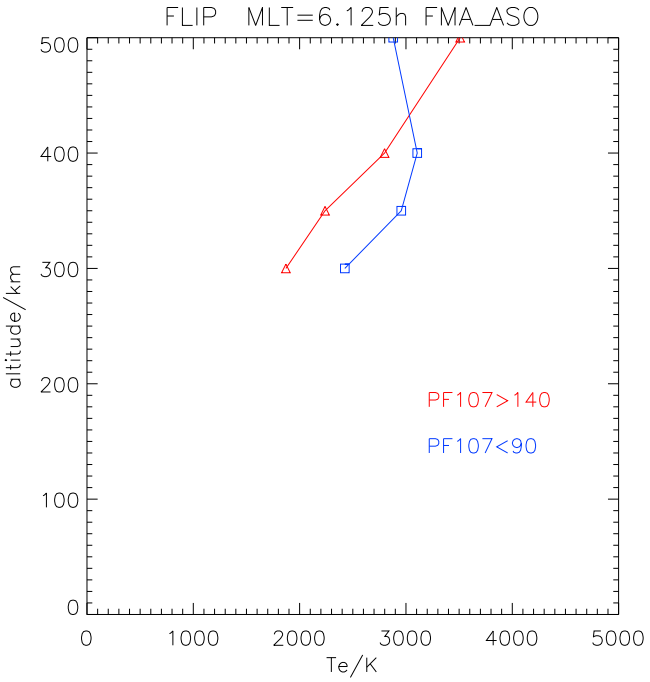

Figure 10. Electron temperature altitude profiles modeled by FLIP at the Jicamarca location. Color and line codes same as Figure 9.

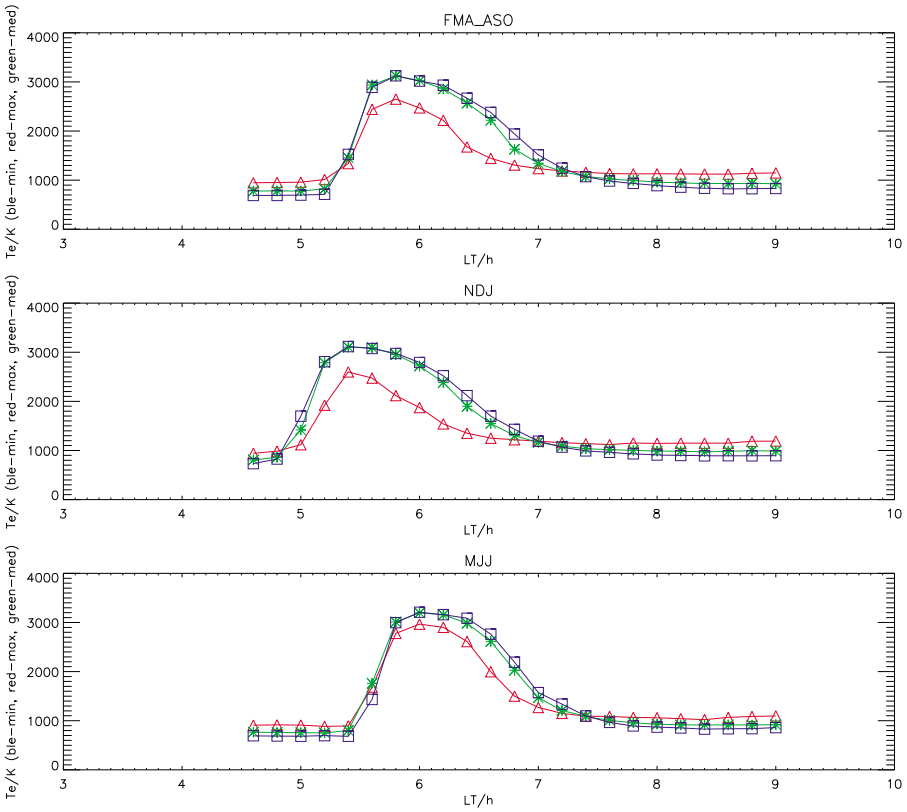

Figure 11. Local time profiles of electron temperatures modeled by FLIP at 350 km altitude and at Jicamarca location. Color and symbols same as Figure 8.

other longitudes. As an example we chose the longitudinal range 85°–115°E, where the declination of the magnetic field is approximately 0°. Figure 12 shows equatorial T_e observations identical to Figure 6 but observed at 85°–115°E. Figure 13 shows the local time, seasonal, and solar flux variations of FLIP model results at 100°E and at 350 km altitude. Since the dip equator is located in the northern hemisphere, the temperatures rise earliest in May, June, July and latest in November, December, January in both data and model. We also observe a longer duration of the morning overshoot for low solar flux indices than for high indices. The model predicts clearly lower T_e morning values at high solar flux levels.

[28] Beside these similarities, differences are also found. The anticorrelation of the morning overshoot with solar activity seems not to be as pronounced as at −75°E. For comparison, between 06 LT and 06.15 LT and at 100°E, the slopes derived from the baseline corrected CHAMP observations are −5.7 K/sfu for NDJ, −1.5 K/sfu for FMA and ASO, and −8.3 K/sfu for MJJ. When inspecting the model results in Figures 11 and 13, we find as well a reduced solar flux dependence at 100°E, e.g., during equinox. Also, following the model, the anticorrelation with solar flux is higher when the dip equator is located in the summer hemisphere than in the winter hemisphere, which are opposite solstices for the two considered longitudes. A further difference has been revealed in Figure 5 where the longitudes −75°E and 100°E are indicated by thin vertical black lines. At low solar activity, the seasonal variation in the morning temperature amplitude is lower at −75°E than at 100°E, but the seasonal variation in the electron densities is larger at −75°E than at 100°E.

[29] FLIP predicts T_e peaks up to 3100 K in December solstice at both longitudes. In June solstice, up to 3400 K at 100°E, but only up to 3200 K at −75°E. In this respect, model and observations give the same temperature trends. Although CHAMP and FLIP showed a negative correlation of the electron temperature morning overshoot in the ionospheric F region at two different longitudinal sectors, we cannot exclude a seasonal/longitudinal variation of this relation.

5. Conclusions

[30] The behavior of the morning overshoot of electron temperature including the dependence on solar flux has been investigated using CHAMP observations and FLIP model results. It is the first time that a continuous data set of T_e has been globally available over 8 years at ionospheric altitudes below 400 km. The CHAMP observations show that the latitudinal shape of the morning overshoot between 05 LT and 07 LT does not vary with season, i.e., the electron temperature maximum is located above the dip equator and does not shift to the winter or summer hemisphere. The morning T_e gradually decreases with increasing dip latitude. The dip latitudinal variation is clearly not due to variation in the local heating or cooling rates because it does not show any relationship to the electron density. The T_e peak at the magnetic equator is due to the decreasing importance of heat conduction as the dip angle becomes smaller with a mini-

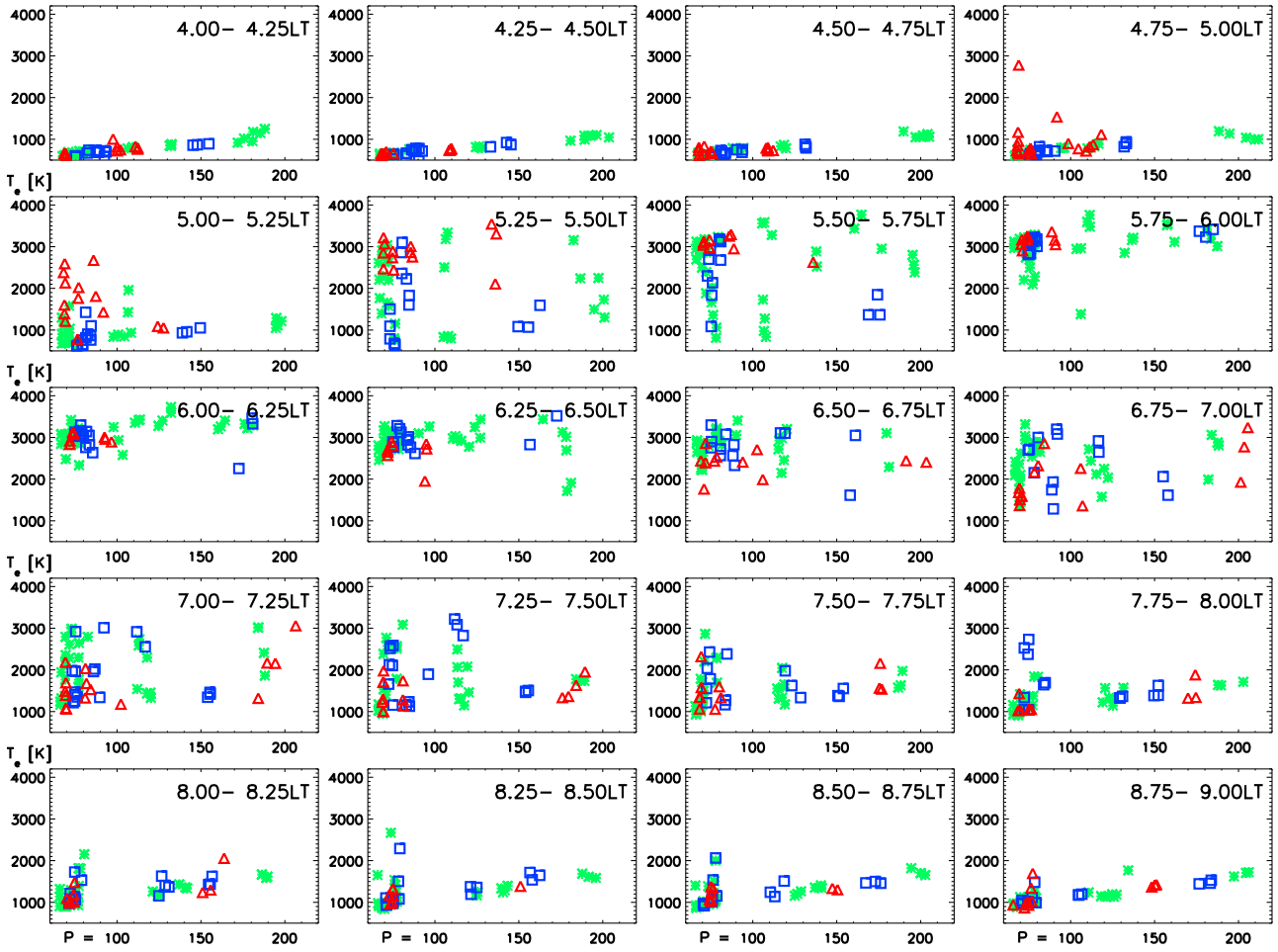

Figure 12. Same as Figure 6 but for longitudes between 85°E and 115°E.

mum in the region of horizontal field lines. This was confirmed by the FLIP model. The longitudinal variation of the morning electron temperature at the magnetic equator follows mainly the longitudinal variation of electron density with correlations of over 90% in June solstice and equinoxes. These findings underline the fact that electron density plays a major role in determining ionospheric electron temperatures at the dip equator where local heating and cooling is important.

[31] The CHAMP data revealed a negative correlation of the amplitude of morning overshoot electron temperature with the solar flux level, which is consistent with the FLIP model simulation results. In both data and model the slopes of the linear regressions between T_e and P are a few K/sfu below zero depending on season and longitude. The model results show that the cooling rate due to collisions with ions, which is quadratic in the electron density, increases more rapidly with solar activity than the combined increases in the heating rate due to the linear increases in the photoelectron flux and the electron density. This is reflected in a decreasing heating/cooling ratio with increasing solar flux.

[32] These findings at the CHAMP altitude are different from the increase of the morning overshoot amplitude with increasing solar flux at altitudes of 600 km, e.g., as observed by the Hinotori satellite. Vertical profiles from Jicamarca radar observations and calculated by the FLIP model show that morning T_e is higher for low solar flux than for high solar flux at F region altitudes, but it is higher for high solar flux above 500 km. We suggest that the lower plasma density and the longer magnetic field lines at Hinotori altitudes alter the balance between local heating and cooling rates and photoelectron transport. This suggestion has to be verified in subsequent modeling studies.

[33] The morning overshoot elevated T_e persist longer when the solar EUV is low, e.g., temperatures observed for $P > 100$ have been found in dayside equilibrium at 08:15 LT, but a significant scatter to high values is still present for data with $P < 100$. At 10 LT all observations at all solar flux levels are in the dayside equilibrium. We suggest that the decreased background plasma density together with the shallower rise of electron and ion densities after sunset are responsible for the longer persistence because the cooling through electron-ion collisions increases more slowly.

[34] Comparing the solar flux dependence at two different longitudes, −75°E and 100°E, showed similar magnitudes of the anticorrelation. A longer persistence of high T_e exists at both sites, both from the data and from the model. Differences between the two longitudes are a weaker anticorrelation at 100°E, and a stronger variation with solar flux when the dip equator lies on the summer hemisphere, which are opposite solstices at the two sites. The amplitude of the morning electron temperature varies by more than 150 K between

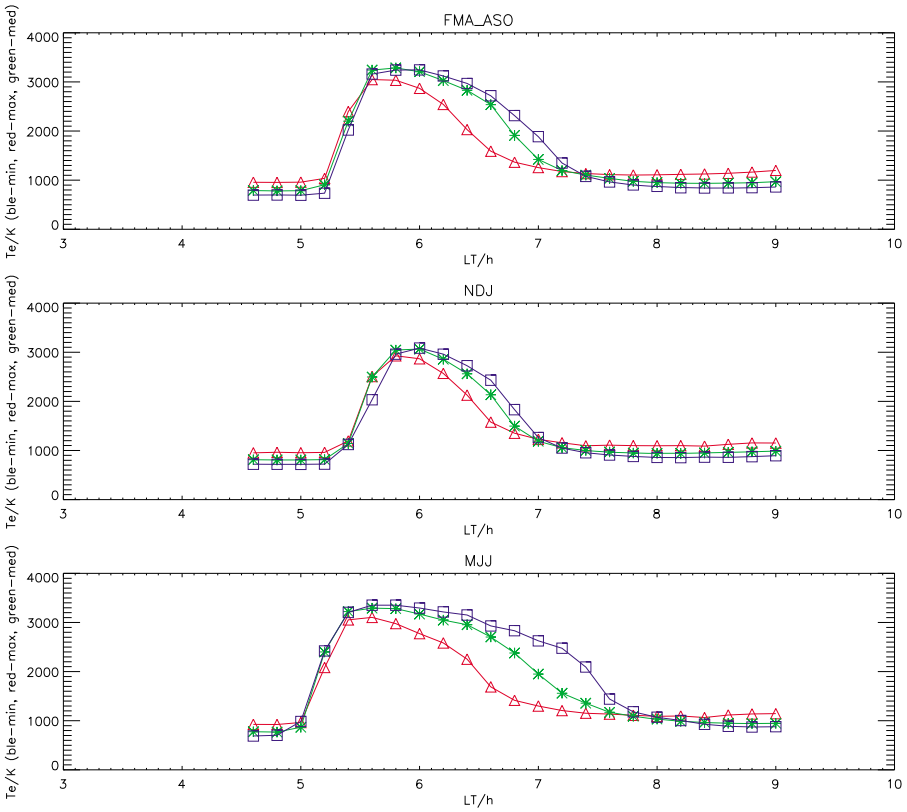

Figure 13. Same as Figure 11 but for 100°E geographic longitude.

winter and summer season at 100°E, but only little variation was found at −75°E. The investigation of the seasonal/longitudinal variation of the ionospheric dependence on solar flux is an interesting topic for ongoing research based on observations and model. In this respect, the upcoming ESA multisatellite mission *Swarm* [*Friis-Christensen et al.*, 2008] will provide extended opportunities, e.g., to monitor local time and height gradients of the morning electron temperature on a day-to-day basis.

[35] **Acknowledgments.** The CHAMP mission is sponsored by the Space Agency of the German Aerospace Center (DLR) through funds of the Federal Ministry of Economics and Technology, following a decision of the German Federal Parliament (grant code 50EE0944). The data retrieval and operation of the CHAMP satellite by the German Space Operations Center (GSOC) is acknowledged. The operation of the incoherent scatter radar and provision of data by the Jicamarca radio observatory is gratefully acknowledged. V.T. was supported by grant P209/10/2086 of the Grant Agency of the Czech Republic. P.G.R. was supported by NASA grant NNX08AF43G.

[36] Robert Lysak thanks the reviewers for their assistance in evaluating this paper.

References

Chao, C. K., S.-Y. Su, J. D. Huba, and K.-I. Oyama (2010), Modeling the presunrise plasma heating in the low- to midlatitudes topside ionosphere, *J. Geophys. Res.*, *115*, A09304, doi:10.1029/2009JA014923.

Cooke, D. L., W. Turnbull, C. Roth, A. Morgan, and R. Redus (2003), Ion drift-meter status and calibration, in *First CHAMP Mission Results for Gravity, Magnetic, and Atmospheric Studies*, edited by C. Reigber, H. Lühr, and P. Schwintzer, pp. 212–219, Springer, Berlin.

Da Rosa, A. V. (1966), The theoretical time dependent thermal behavior of the ionosphere electron gas, *J. Geophys. Res.*, *7*, 4107–4120.

Evans, J. V. (1965), Cause of the midlatitude evening increase in f_oF_2, *J. Geophys. Res.*, *70*, 1175–1185.

Farley, B., D. Balsey, R. Woodman, and J. McClure (1970), Equatorial spread F: Implications of VHF radar observations, *J. Geophys. Res.*, *75*, 7199–7216.

Farley, D. T. (1991), Early incoherent scatter observations at Jicamarca, *J. Atmos. Terr. Phys.*, *53*, 665–675.

Farley, D. T., J. P. McClure, D. L. Sterling, and L. J. Green (1967), Temperature and composition of the equatorial ionosphere, *J. Geophys. Res.*, *72*, 5837–5851.

Fejer, B. G., J. W. Jensen, and S.-Y. Su (2008), Quiet-time equatorial *F* region vertical plasma drift model derived from ROCSAT-1 observations, *J. Geophys. Res.*, *113*, A05304, doi:10.1029/2007JA012801.

Fox, J. L., and K. Y. Sung (2001), Solar activity variations of the Venus thermosphere/ionosphere, *J. Geophys. Res.*, *106*, 21,305–21,335.

Friis-Christensen, E., H. Lühr, D. Knudsen, and R. Haagmans (2008), Swarm - An Earth observation mission investigating geospace, *Adv. Space Res.*, *41*(1), 210–216, doi:10.1016/j.asr.2006.10.008.

Geisler, J. E., and S. A. Bowhill (1965), Exchange of energy between the ionosphere and the protonosphere, *J. Atmos. Terr. Phys.*, *27*, 457–474.

Hedin, A. E. (1987), MSIS-86 thermosphere model, *J. Geophys. Res.*, *92*, 4649–4662.

Itikawa, Y. (1975), Electron-ion energy transfer rate, *J. Atmos. Terr. Phys.*, *37*, 1601–1602.

Kakinami, Y., N. Balan, J. Y. Liu, and K.-I. Oyama (2010), Predawn ionospheric heating observed by Hinotori satellite, *J. Geophys. Res.*, *115*, A01304, doi:10.1029/2009JA014334.

Lee, J. S., J. P. Doering, T. A. Potemra, and L. H. Brace (1980), Measurements of the ambient photoelectron spectrum from atmosphere explorer: I. AE-E measurements below 300 km during solar minimum conditions, *Planet. Space Sci.*, *28*, 947–971.

Lei, J., R. G. Roble, W. Wang, B. A. Emery, and S.-R. Zhang (2007), Electron temperature climatology at Millstone Hill and Arecibo, *J. Geophys. Res.*, *112*, A02302, doi:10.1029/2006JA012041.

Liu, H., C. Stolle, M. Förster, and S. Watanabe (2007), Solar activity dependence of the electron density at 400 km at equatorial and low latitudes observed by CHAMP, *J. Geophys. Res.*, *112*, A11311, doi:10.1029/2007JA012616.

Liu, L., W. Wan, B. Ning, and M.-L. Zhang (2009), Climatology of the mean total electron content derived from GPS global ionospheric maps, *J. Geophys. Res.*, *114*, A06308, doi:10.1029/2009JA014244.

McNamara, L. F., D. L. Cooke, C. E. Valladares, and B. W. Reinisch (2007), Comparison of CHAMP and Digisonde plasma frequencies at Jicamarca, Peru, *Radio Sci.*, *42*, RS2005, doi:10.1029/2006RS003491.

McNamara, L. F., J. M. Retterer, C. R. Baker, G. J. Bishop, D. L. Cooke, C. J. Roth, and J. A. Welsh (2010), Longitudinal structure in the CHAMP electron densities and their implications for global ionospheric modeling, *Radio Sci.*, *45*, RS2001, doi:10.1029/2009RS004251.

Müller, S., H. Lühr, and S. Rentz (2009), Solar and magnetospheric forcing of the low latitude thermospheric mass density as observed by CHAMP, *Ann. Geophys.*, *27*, 2087–2099.

Nagy, A., and P. Banks (1970), Photoelectron fluxes in the ionosphere, *J. Geophys. Res.*, *75*, 6260–6270.

Otsuka, Y., S. Kawamarura, N. Balan, S. Fukao, and G. J. Bailey (1998), Plasma temperature variations in the ionosphere over the middle and upper atmosphere radar, *J. Geophys. Res.*, *103*, 20,705–20,713.

Oyama, K.-I., N. Balan, S. Watanabe, T. Takahashi, F. Isoda, G. J. Bailey, and H. Oya (1996), Morning overshoot of T_e enhanced by downward plasma drift in the equatorial topside ionoshere, *J. Geomag. Geoelectr.*, *48*, 959–966.

Picone, J. M., A. E. Hedin, D. P. Drob, and A. C. Aikin (2002), NRLMSISE-00 empirical model of the atmosphere: Statistical comparisons and scientific issues, *J. Geophys. Res.*, *107*(A12), 1468, doi:10.1029/2002JA009430.

Reigber, C., H. Lühr, and P. Schwintzer (2002), CHAMP mission status, *Adv. Space Res.*, *30*, 129–134.

Ren, Z., W. Wan, L. Liu, B. Zhao, Y. Wei, X. Yue, and R. A. Heelis (2008), Longitudinal variations of electron temperature and total ion density in the sunset equatorial topside ionosphere, *Geophys. Res. Lett.*, *35*, L05108, doi:10.1029/2007GL032998.

Richards, P. G. (1986), Thermal electron quenching of N(^{2}D): Consequences for the ionospheric photoelectron flux and the thermal electron temperature, *Planet. Space Sci.*, *34*, 689–694.

Richards, P. G. (2001), Seasonal and solar cycle variations of the ionospheric peak electron density: Comparison of measurement and models, *J. Geophys. Res.*, *106*, 12,803–12,819.

Richards, P. G. (2002), Ion and neutral density variations during ionospheric storms in September 1974: Comparison of measurement and models, *J. Geophys. Res.*, *107*(A11), 1361, doi:10.1029/2002JA009278.

Richards, P. G., and W. K. Peterson (2008), Measured and modeled backscatter of ionospheric photoelectron fluxes, *J. Geophys. Res.*, *113*, A08321, doi:10.1029/2008JA013092.

Richards, P. G., and D. G. Torr (1985), The altitude variation of the ionospheric photoelectron flux: A comparison of theory and measurement, *J. Geophys. Res.*, *90*, 2877–2884.

Richards, P. G., J. A. Fennelly, and D. G. Torr (1994), EUVAC: A solar EUV flux model for aeronomic calculations, *J. Geophys. Res.*, *99*, 8981–8992.

Richards, P. G., T. N. Woods, and W. K. Peterson (2006), HEUVAC: A new high resolution solar EUV proxy model, *Adv. Space Res.*, *37*, 315–322, doi:10.1016/j.asr.2005.06.031.

Rother, M., K. Schlegel, H. Lühr, and D. L. Cooke (2010), Validation of CHAMP electron temperature measurements by incoherent scatter radar data, *Radio Sci.*, *45*, RS6020, doi:10.1029/2010RS004445.

Scherliess, L., and B. G. Fejer (1999), Radar and satellite global equatorial *F* region vertical drift model, *J. Geophys. Res.*, *104*, 6829–6842.

Schunk, R. W., and A. F. Nagy (1978), Electron temperatures in the *F* region of the ionosphere: Theory and observations, *Rev. Geophys.*, *16*, 355–399.

Stolle, C., C. Manoj, H. Lühr, S. Maus, and P. Alken (2008), Estimating the day time Equatorial Ionization Anomaly strength from electric field proxies, *J. Geophys. Res.*, *113*, A09310, doi:10.1029/2007JA012781.

Su, Y. Z., K.-I. Oyama, G. J. Bailey, T. Takahashi, and S. Watanabe (1995), Comparison of satellite electron density and temperature measurements at low latitudes with a plasmasphere-ionosphere model, *J. Geophys. Res.*, *100*, 14,591–14,605.

Torr, M. R., D. G. Torr, P. G. Richards, and S. P. Yung (1995), Mid- and low-latitude model of thermospheric emissions, 1, $O_+(^2P)$ 7320 Å and $N_2(2P)$ 3371 Å, *J. Geophys. Res.*, *95*, 21,147–21,168.

Truhlík, V., L. Třísková, and J. Šmilauer (2001), Improved electron temperature model and comparison with satellite data, *Adv. Space Res.*, *27*, 101–109.

Truhlík, V., L. Třísková, and J. Šmilauer (2003), Response of outer ionoshere electron temperature and density to changes in solar activity, *Adv. Space Res.*, *31*, 697–700.

Truhlík, V., D. Bilitza, and L. Třísková (2009), Latitudinal variation of the topside electron temperature at different levels of solar activity, *Adv. Space Res.*, *44*, 693–700.

Watanabe, S., and K.-I. Oyama (1996), Effects of neutral wind on the electron temperature at a height of 600 km in the low latitude region, *Ann. Geophys.*, *14*, 290–296.

Watanabe, S., K.-I. Oyama, and M. A. Abdu (1996), Computer simulations of electron and ion densities and temperatures in the equatorial *F* region and comparison with Hinotori results, *J. Geophys. Res.*, *100*, 14,581–14,590.

H. Liu, Research Institute for Sustainable Humanosphere, Kyoto University, Kyoto 611-0011, Japan.

H. Lühr, Helmholtz Centre Potsdam, GFZ German Research Centre for Geosciences, Telegrafenberg, D-14473 Potsdam, Germany.

P. G. Richards, Department of Physics and Astronomy, George Mason University, Fairfax, VA 22030, USA.

C. Stolle, National Space Institute, Technical University of Denmark, Juliane Maries vej 30, DK-2100 Copenhagen, Denmark. (cst@space.dtu.dk)

V. Truhlík, Institute of Atmospheric Physics, Academy of Sciences of the Czech Republic, Boční II 1401, 141 31 Praha 4, Czech Republic.